Non-line-of-sight imaging in the presence of scattering media using phasor fields

PABLO LUESIA[1*], MIGUEL CRESPO[1*], ADRIAN JARABO[1], AND ALBERT REDO-SANCHEZ[1]

[1] *Universidad de Zaragoza, I3A*
[*] *Joint first authors*

Compiled December 17, 2025

Non-line-of-sight (NLOS) imaging aims to reconstruct scenes that are partially or completely occluded. Recent approaches have demonstrated high-quality reconstructions in complex scenes with arbitrary reflectance, occlusions, and significant multi-path. However, previous works have focused on surface scattering only, which reduces its generality in more challenging scenarios such as scenes submerged in scattering media. In this work, we investigate how current state-of-the-art NLOS imaging methods, based on phasor fields, perform at reconstructing occluded scenes submerged in scattering media. We empirically analyze the performance of phasor fields in synthetic scenes in the presence of scattering media, and show that phasor fields can reconstruct complex hidden scenes even in the presence of thick scattering media. We also apply the method on real scenes, showing that it performs similarly as recent diffuse optical tomography methods.

OCIS codes: (010.1350) Backscattering; (150.0155) Machine vision optics; (110.1758) Computational imaging.

http://dx.doi.org/10.1364/ao.XX.XXXXXX

Recent advances in transient imaging [1] using ultrafast sensors have opened a wide range of novel imaging modalities, including the ability of imaging fully or partially occluded objects, or *non-line-of-sight (NLOS) imaging* [2–7] NLOS imaging has a large body of applications, including medical imaging, autonomous driving, or surveillance and security, among others.

NLOS imaging aims to recover hidden scenes by using the light scattered from a visible secondary surface, or *relay wall* [8]. Most previous NLOS imaging approaches are based on time-resolved information and filtered backprojection using heuristic filters [2, 9, 10], or inverting simplistic ad-hoc light transport models [3, 6, 7, 11]. Unfortunately, these approaches do not properly deal with the challenges resulting from multiple scattering, anisotropic reflectance, occlusions, and clutter in the hidden scene. Recent wave-based models for NLOS imaging [4, 5, 12] have overcome some of these limitations by posing NLOS imaging as a *virtual* wave-propagation problem, effectively transforming NLOS imaging into a *virtual* line-of-sight (LOS) problem. These algorithms have allowed NLOS imaging of real-world complex scenes at the meter scale.

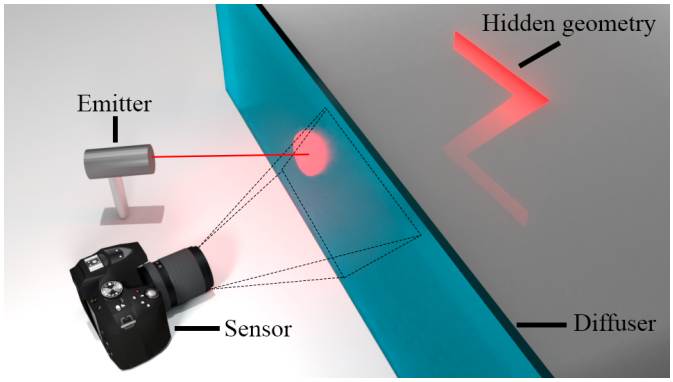

Fig. 1. Scene setup. We aim to image a scene hidden behind a diffuser, with the hidden scene submerged in a scattering medium (e.g., smoke or fog).

All these techniques assume that light travels in an environment without the presence of any scattering media. This assumption limits the applicability of NLOS imaging to scenarios in which the presence of scattering media (e.g., smoke or fog) might be significant, including driving through fog or medical endoscopic imaging. Imaging through scattering media is challenging even in LOS setups, where many techniques have been proposed, for example, using optical coherence tomography (OCT) [13–16], diffuse optical tomography (DOT) [17, 18], sparse coding in combination with time-of-flight measurements [19, 20], structured light [21], coherent light modulation using spatial light modulators [22], or polarization [23–26].

In this letter, we empirically analyze the performance of NLOS imaging methods in scenes with scattering media (see Figure 1). Given the amount of incoherent light due to scattering, we cannot rely on traditional inversion methods for NLOS imaging. Instead, we leverage recent advances on wave-based NLOS imaging, and in particular on the *phasor fields* framework proposed by Liu and colleagues [4]. This framework allows us creating virtual illumination and sensors on the visible surfaces, resulting in robust reconstruction of multiple incoherent scattered light sources [27–29]. We demonstrate reconstructions of NLOS scenes in the presence of scattering media of increasing density, showing that *phasor fields* framework is a feasible tool for reconstructing scenes in very challenging visibility conditions,

using a single-frequency laser grid for illumination on a single plane, compared to OCT and DOT techniques.We hope this work will bridge the gap between NLOS imaging and the capability to see through scattering media and foster new avenues of work in the NLOS imaging field.

NLOS imaging using *phasor fields* [4] is based on the observation that, by convolving a time-resolved optical carrier with a monochromatic phasor, we can model the propagation of this virtual phasor using a Rayleigh-Sommerfeld Diffraction (RSD)-like operator. The immediate consequence of this observation is that we can use well-known tools from Fourier optics to model sophisticated virtual imaging and illumination systems. Therefore, by measuring the impulse linear light transport matrix of the hidden scene $H(\mathbf{x}_p \rightarrow \mathbf{x}_c, t)$, we can pose the NLOS imaging problem as a *virtual* LOS setup. Let us define the phasor $\mathcal{P}_\omega(\mathbf{x}, t)$ at point $\mathbf{x}$, time t, and with frequency ω as

$$\mathcal{P}_\omega(\mathbf{x}, t) \equiv \mathcal{P}_{0,\omega}(\mathbf{x}) e^{i\omega t}, \tag{1}$$

with $\mathcal{P}_{0,\omega}(\mathbf{x})$ and $e^{i\omega t}$ being the intensity and phase at the instant t of the phasor. We can model the propagation from a surface S to a point $\mathbf{x}_d \in D$ of this virtual wave field $\mathcal{P}_\omega(\mathbf{x}, t)$ as

$$\mathcal{P}_\omega(\mathbf{x}_d, t) = \gamma \int_S \mathcal{P}_\omega(\mathbf{x}_s, t) \frac{e^{ik|\mathbf{x}_d - \mathbf{x}_s|}}{|\mathbf{x}_d - \mathbf{x}_s|} d\mathbf{x}_s, \tag{2}$$

where $\gamma \approx 1/\mid \langle S \rangle - \mathbf{x}_d \mid$ is an attenuation factor, k is the wavelength number ($k = 2\pi/\lambda$), being λ the wavelength of the frequency, ω is the frequency of the monochromatic component, $\mathbf{x}_s \in S$, and $\mathbf{x}_d \in D$. Eq. (2) has the form of a RSD operator. In the following, we remove the frequency dependence from the phasor and consider only monochromatic phasors. Non-monochromatic phasors can be constructed as the superposition of the monochromatic phasor components.

In order to image a hidden scene from a virtual camera with the aperture placed at surface C, we first need to compute the incoming phasor field on the virtual sensor $\mathcal{P}(\mathbf{x}_c, t)$ with $\mathbf{x}_c \in C$ as a function of a phasor $\mathcal{P}(\mathbf{x}_p, t)$ in the virtual emitter on surface P. This is computed by leveraging the linearity and time-invariance of light transport, using the impulse response of the hidden scene $H(\mathbf{x}_p \rightarrow \mathbf{x}_c, t)$ to compute $\mathcal{P}(\mathbf{x}_c, t)$ as

$$\mathcal{P}(\mathbf{x}_c, t) = \int_P \mathcal{P}(\mathbf{x}_p, t) \star H(\mathbf{x}_p \rightarrow \mathbf{x}_c, t) d\mathbf{x}_p, \tag{3}$$

where $\star$ denotes the convolution operator. Finally, to generate the image of the hidden scene $I(\mathbf{x}_v)$ as seen from the virtual sensor, with $\mathbf{x}_v$ the point being reconstructed, an image formation model $\Phi(\cdot)$ is applied over $\mathcal{P}(\mathbf{x}_c, t)$ as

$$I(\mathbf{x}_v) = \Phi\left(\mathcal{P}(\mathbf{x}_c, t)\right). \tag{4}$$

The image-formation function $\Phi(\cdot)$ depends on the type of imaging system (details in [4]). In our work, we use a virtual time-gated camera, by setting the emitter phasor $\mathcal{P}(\mathbf{x}_p, t)$ and image formation function $\Phi(\mathcal{P}(\mathbf{x}_c, t))$ to

$$\mathcal{P}(\mathbf{x}_p, t) = e^{i\omega(t - \frac{1}{c}|\mathbf{x}_v - \mathbf{x}_p|)} e^{-\frac{(t - t_0 - \frac{1}{c}|\mathbf{x}_v - \mathbf{x}_p|)^2}{2\sigma^2}} \quad \text{and} \tag{5}$$

$$\Phi(\mathcal{P}(\mathbf{x}_c, t)) = \left| \mathcal{R}_{\mathbf{x}_v}\left(\mathcal{P}(\mathbf{x}_c, -\frac{1}{c}|\mathbf{x}_v - \mathbf{x}_c|)\right)\right|^2, \tag{6}$$

where c is the speed of light in vacuum and $\mathcal{R}_{\mathbf{x}_v}$ is the RSD operator from $\mathbf{x}_v$ to $\mathbf{x}_c$, and σ is the width of the virtual illumination pulse used to focus on the specific voxel $\mathbf{x}_v$. Thus, the virtual camera is focused to each particular voxel, while the virtual illumination acts as a single pulsed point source.

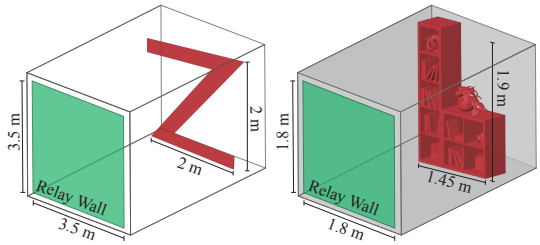

Fig. 2. Simulated scenes. We use two simulated scenes in our experiments: (Left) a scene consisting of a single planar letter behind the diffuser (in green), and (right) a scene of a closed room (walls in gray) with a shelf (red) on the back wall.

While phasor fields have demonstrated very effective at reconstructing NLOS scenes in standard ambient conditions, little has been investigated in relation to its performance in reconstructing scenes submerged in scattering media, which results in more challenging visibility conditions for the experimental equipment operating in the visible range.

In the following, we analyze the performance of phasor fields in scenes hidden behind a visible diffuser and submerged in scattering media of increasing density (see Figure 1). The scene setup differs with traditional NLOS scene configurations, where the *relay wall* reflects the light into the scene generating a geometry for looking around corners. Our *relay wall* is the diffuser, which transmits the light into and out of the scene. Note that the setup is equivalent to a LOS setup through heterogeneous media, using the diffuser as occluder.

Experimental design. We perform our experiment using both simulated data and captured experimental data. The simulated scenes allow us to easily control the properties of the scattering media, while the experimental data allows us to assess the behavior in a real world scenario.

For **simulation,** we use two different scenes (see Figure 2): A simple scene with a planar Z-letter in front of the diffuser at a distance of 2 meters on a free space, and a more complex scene containing an enclosed room with a shelf located 1.8 meters away from the diffuser. The Z-LETTER scene allows us to study how the medium affects visibility in the phasor-fields domain. On the other hand, the SHELF scene results into a more challenging scenario due to feature occlusions and multi-path illumination. It serves us to validate the results derived from the Z-LETTER scene in more complex scenarios.

We characterize the scattering media by using their bulk optical parameters. In particular, we use the extinction coefficient $\mu_t = \mu_a + \mu_s$ [m^{-1}], and single scattering albedo $\alpha = \mu_s/\mu_t$ [unitless], with μ_a and μ_s the absorption and scattering coefficients [m^{-1}], respectively. Intuitively, the extinction is related with medium density and the single scattering albedo with the amount of scattering.

We model the directionality of the scattering by using the Henyey-Greenstein [30] phase function, which models the directionality using the anisotropy factor $g \in (-1, 1)$, where $g > 0$, $g = 0$, and $g < 0$ model forward, isotropic, and backward scattering respectively. Unless stated otherwise, we assume an isotropic phase function $g = 0$ and homogeneous media.

We use a publicly available transient renderer software [31] to compute the impulse response $H(\mathbf{x}_p \rightarrow \mathbf{x}_c, t)$ of the hidden

scenes. We compute each impulse response for 128^2 laser positions $\mathbf{x}_p$ equally spaced in a grid along the visible diffuser, and captured in a single SPAD point $\mathbf{x}_c$. The temporal resolution is 4096 bins, each with a temporal resolution of about 3 ms.

We use the **experimental** data captured by Lindell and Wetzstein [17], that captures the impulse response of a scene hidden behind a thick diffuser using a confocal laser and SPAD sensor. They measured 32^2 equally-spaced positions $\mathbf{x}_c$ using a confocal configuration ($\mathbf{x}_c = \mathbf{x}_p$). Note that the scenes are not submerged in scattering media, but in this case the diffuser acts as a highly scattering medium, resulting into a similar problem to the one described above.

Reconstruction. We reconstruct a volumetric representation of the scenes by sequentially focusing the virtual imaging system on each voxel. The voxelization resolution is $73 \times 59 \times 73$ for the Z-LETTER scene, 142^3 for the SHELF scene, and 32^3 for all the CAPTURED scenes from Lindell and Wetzstein. The reconstruction time scales linearly with the voxelization resolution: On an Intel Xeon E5 with 256 GB RAM, the Z-LETTER scene took 29 seconds to reconstruct, the SHELF scene 254 seconds, and each CAPTURED scenes 5 seconds, on average. We use the Matlab solver provided by the authors [4].

Following Liu et al. [4], we set the reconstruction Gaussian pulse Eq. (5) with a central wavelength $\lambda = 4\,\Delta_c$ with Δ_c, being the distance between sampled points on the relay wall. The pulse has a complete width of 4λ in the simulated data reconstructions, and 8λ in the experimental data reconstructions ($\sigma = 4\lambda/6$ and $\sigma = 8\lambda/6$ respectively). Similar to LOS Fourier optics, the wavelength defines the maximum resolution of the reconstruction. Later we analyze the effect of λ in the reconstruction and how it can be exploited for deeper penetration.

For visualization, we remove the contribution of the extinction of medium by filtering the final reconstruction in post-process. We exploit the spatial information of the voxels, as well as the (known) properties of the medium, and apply the following scale factor $K(\mathbf{x}_v)$ for each voxel

$$K(\mathbf{x}_v) = (1 - \alpha e^{-|\mathbf{x}_v - \mathbf{x}_c|\,\alpha})/(e^{-|\mathbf{x}_v - \mathbf{x}_c|\,\mu_t}), \qquad \textbf{(7)}$$

which depends on the bulk optical properties of the medium. On a real-world scenario, the media properties are usually unknown, but could be obtained from the measurements using inverse scattering [32].

Analysis. Figure 3b shows the results of phasor fields when reconstructing the simple Z-LETTER scene as a function of different media densities (its extinction coefficient μ_t) and relative amount of scattering (scattering albedo α). For low scattering albedo, as the media thickness increases, the amplitude of the signal is attenuated, though the coherence remains, so it is still possible to reconstruct a sharp image. In contrast, a higher single scattering albedo results into less coherence and, therefore, into the loss of high frequency information.

Figure 3c shows the effect on the reconstructions of the phase function's anisotropy. For forward scattering, the phasor penetrates deeper into the medium, whereas backward scattering results into more scattering near the virtual camera and, therefore, poorer visibility conditions.

Now we analyze the effect of the phasor wavelength λ on the reconstruction and how this allows for deeper penetration in the medium. Figure 4 compares the reconstruction in a high scattering medium ($\mu_t = 1\ m^{-1}$, $\alpha = 0.87$) for increasing λ. In particular, we double and triple the optimal central wavelength defined by $\lambda = 4$ and Δ_c. This results into a resolution loss, visible as smoother reconstructions. However, we still can recover the geometry hidden by the scattering in the medium more clearly by increasing the wavelength.

We also analyze how our experiments extrapolate to scenes with significantly more complexity. Figure 5 shows the NLOS reconstruction of the SHELF scene. The scene contains surface-to-surface multi-path, and multiple scattering in the medium. This results in larger indirect contribution to the medium, thus resulting in more challenging visibility conditions. As our results show, even for relatively thick media we can reconstruct such complex scene with good quality.

Finally, we analyze the phasor fields method on the confocal data captured by Lindell and Wetzstein [17]. Similar to us, their method is based on an inversion technique used for NLOS imaging (f-k migration [5]). The results are on-pair with Lindell and Wetzstein's method, without any modification of the phasor fields framework, demonstrating its flexibility even in challenging conditions.

In conclusion, we have empirically analyzed the performance of phasor fields in complex visibility conditions i.e. in the presence of scattering media. We have leveraged the capability of phasor fields of transforming a NLOS problem into a virtual LOS one, in which the scattering media acts as an additional occluder. Our empirical analysis demonstrates that it is feasible to reconstruct NLOS scenes in very challenging visibility conditions under a wide range of media properties. Moreover, we have also shown that, by increasing the reconstruction wavelength, we can partially remove the contribution of the medium at the cost of a resolution loss. However, our work is limited by the same challenges present in LOS systems and, therefore, we can expect that off-the-shelf phasor fields for very dense scattering media will not be optimal at reconstructing a hidden scene. However, given the flexibility of phasor fields for developing virtual complex optical systems, a possible avenue of work is to translate current LOS methods for vision through scattering media into the phasor field framework.

Funding. Left blank during review.

Disclosures. The authors declare no conflicts of interest.

Data Availability Statement. Left blank during review.

REFERENCES

1. A. Jarabo, B. Masia, J. Marco, and D. Gutierrez, Vis. Informatics **1** (2017).
2. A. Velten, T. Willwacher, O. Gupta, A. Veeraraghavan, M. G. Bawendi, and R. Raskar, Nat. Commun. **3**, 745 (2012).
3. M. O'Toole, D. B. Lindell, and G. Wetzstein, Nature. **555**, 338 (2018).
4. X. Liu, I. Guillén, M. La Manna, J. H. Nam, S. A. Reza, T. H. Le, A. Jarabo, D. Gutierrez, and A. Velten, Nature. **572**, 620 (2019).
5. D. B. Lindell, G. Wetzstein, and M. O'Toole, ACM Trans. Graph. **38**, 116 (2019).
6. S. Xin, S. Nousias, K. N. Kutulakos, A. C. Sankaranarayanan, S. G. Narasimhan, and I. Gkioulekas, "A theory of Fermat paths for non-line-of-sight shape reconstruction," in *IEEE CVPR*, (2019), pp. 6800–6809.
7. J. Iseringhausen and M. B. Hullin, ACM Trans. Graph. **39**, 1 (2020).
8. T. Maeda, G. Satat, T. Swedish, L. Sinha, and R. Raskar, arXiv preprint arXiv:1910.05613 (2019).
9. M. Laurenzis and A. Velten, Opt. Eng. **53**, 023102 (2014).
10. V. Arellano, D. Gutierrez, and A. Jarabo, Opt. Express **25**, 11574 (2017).
11. F. Heide, M. O'Toole, K. Zang, D. B. Lindell, S. Diamond, and G. Wetzstein, ACM Trans. Graph. **38**, 22 (2019).

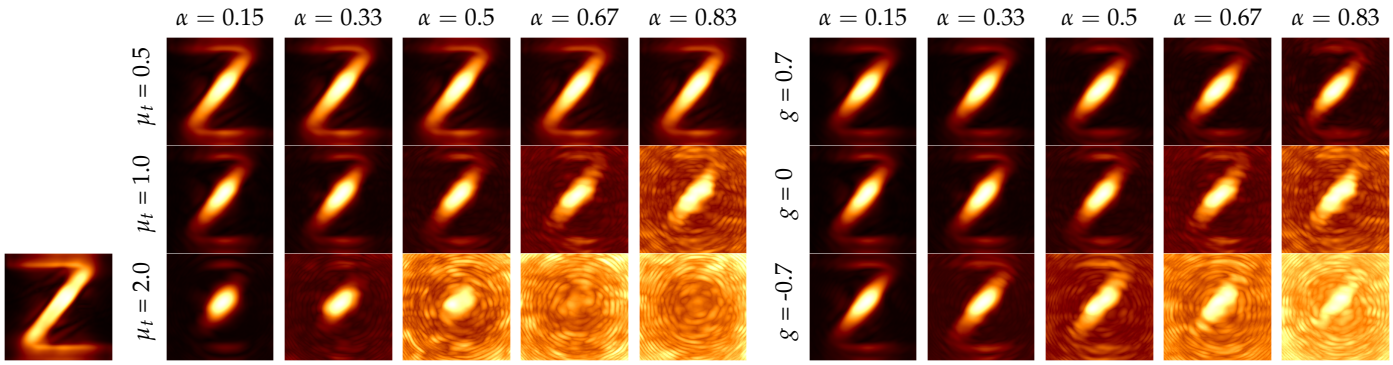

(a) $\mu_t = 0$ **(b)** Extinction coefficient μ_t vs. single scattering albedo α **(c)** Single scattering albedo $alpha$ vs. phase function anisotropy g

Fig. 3. Reconstructions using phasor fields of the Z-LETTER scene. a scene without any media. b reconstructions in the presence of scattering media for varying extinction μ_t (in m^{-1}) and single scattering albedo α [unitless]. c reconstructions in the presence of scattering media, for fixed extinction $\mu_t = 1\ m^{-1}$, varying single scattering albedo α (unitless) and phase function's anisotropy g (rows, unitless). Phasor fields is able reconstructs the Z-LETTER surface even with very scattering media.

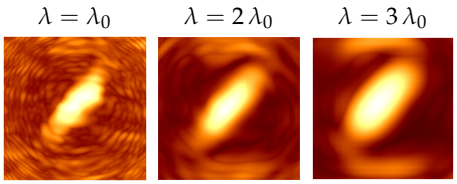

Fig. 4. Reconstructions with phasor fields of the Z-LETTER scene in the presence of a scattering medium ($\mu_t = 1m^{-1}$ and $\alpha = 0.83$) for increasing wavelength λ, with baseline $\lambda_0 = 4\Delta_c$ and $\Delta_c = 0.11m$. Higher values of λ result into deeper penetration through the medium, at the cost of lower spatial resolution on the reconstruction.

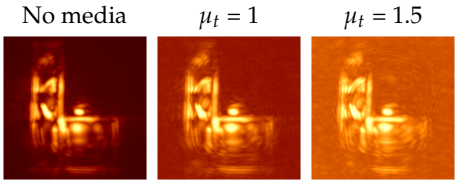

Fig. 5. NLOS reconstruction of the SHELF scene in the presence of media of increasing density: From left to right, $\mu_t = 0$ (no media), $\mu_t = 1$, and $\mu_t = 1.5$. In all cases, the scattering albedo is fixed to $\alpha = 0.5$.

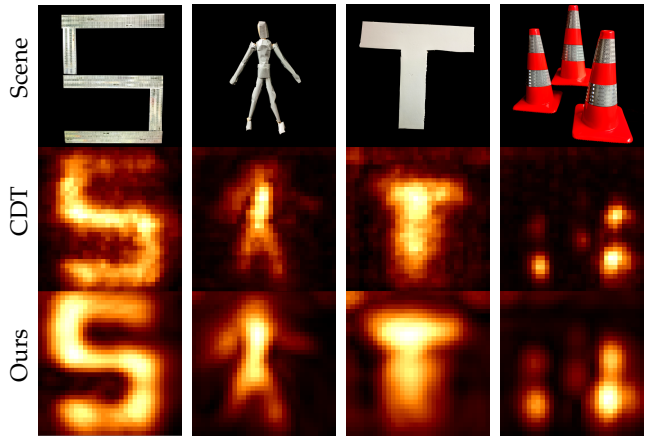

Fig. 6. Reconstructions of real world measures scenarios. Each column represents a different scene. Top: photographs of the scenes behind the diffuser. Middle: Lindell and Wetzstein reconstructions [17] (CDT). Bottom: our reconstructions using phasor fields. The higher-frequency of CDT is related to the deconvolution to compensate scattering at the diffuser.

12. X. Liu, S. Bauer, and A. Velten, Nat. Commun. **11**, 1 (2020).
13. D. Huang, E. A. Swanson, C. P. Lin, J. S. Schuman, W. G. Stinson, W. Chang, M. R. Hee, T. Flotte, K. Gregory, C. A. Puliafito *et al.*, Science. **254**, 1178 (1991).
14. P. N. d. Outer, A. Lagendijk, and T. M. Nieuwenhuizen, J. Opt. Soc. Am. A **10**, 1209 (1993).
15. P. Han, G. Cho, and X.-C. Zhang, Opt. Lett. **25**, 242 (2000).
16. A. Gibson, J. Hebden, and S. R. Arridge, Phys. Med. Biol. **50**, R1 (2005).
17. D. B. Lindell and G. Wetzstein, Nat. Commun. **11**, 1 (2020).
18. A. Lyons, F. Tonolini, A. Boccolini, A. Repetti, R. Henderson, Y. Wiaux, and D. Faccio, Nat. Photonics **13**, 575 (2019).
19. G. Satat, M. Tancik, and R. Raskar, 2018 IEEE Int. Conf. on Comput. Photogr. (ICCP) pp. 1–10 (2018).
20. F. Heide, L. Xiao, A. Kolb, M. B. Hullin, and W. Heidrich, Opt. Express **22**, 26338 (2014).
21. S. G. Narasimhan, S. K. Nayar, B. Sun, and S. J. Koppal, "Structured light in scattering media," in *IEEE ICCV,* , vol. 1 (2005), pp. 420–427.
22. I. M. Vellekoop and A. Mosk, Opt. Lett. **32**, 2309 (2007).
23. S. Demos and R. Alfano, Appl. Opt. **36**, 150 (1997).
24. Y. Y. Schechner, S. G. Narasimhan, and S. K. Nayar, "Instant dehazing of images using polarization," in *IEEE CVPR,* , vol. 1 (2001).
25. T. Treibitz and Y. Y. Schechner, IEEE Trans. Pattern Anal. Mach. Intell. **31**, 385 (2008).
26. R. Wu, A. Jarabo, J. Suo, F. Dai, Y. Zhang, Q. Dai, and D. Gutierrez, Opt. Lett. **43** (2018).
27. S. A. Reza, M. La Manna, S. Bauer, and A. Velten, Opt. Express **27**, 32587 (2019).
28. J. Dove and J. H. Shapiro, Opt. Express **27**, 18016 (2019).
29. J. A. Teichman, Opt. Express **27**, 27500 (2019).
30. L. Henyey and J. Greenstein, The Astrophys. J. **93**, 70 (1941).
31. A. Jarabo, J. Marco, A. Muñoz, R. Buisan, W. Jarosz, and D. Gutierrez, ACM Trans. Graph. **33** (2014).
32. I. Gkioulekas, A. Levin, and T. Zickler, "An evaluation of computational imaging techniques for heterogeneous inverse scattering," in *European Conference on Computer Vision,* (Springer, 2016), pp. 685–701.